

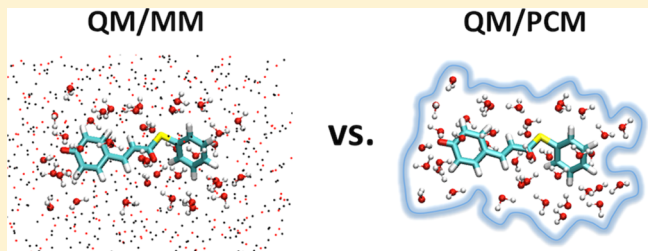
Convergence of Excitation Energies in Mixed Quantum and Classical Solvent: Comparison of Continuum and Point Charge Models

Makenzie R. Provorse, Thomas Peev, Chou Xiong, and Christine M. Isborn*

Chemistry and Chemical Biology, University of California at Merced, Merced, California 95343, United States

 Supporting Information

ABSTRACT: Mixed quantum mechanical (QM)/classical methods provide a computationally efficient approach to modeling both ground and excited states in the condensed phase. To accurately model short-range interactions, some amount of the environment can be included in the QM region, whereas a classical model can treat long-range interactions to maintain computational affordability. The best computational protocol for these mixed QM/classical methods can be determined by examining convergence of molecular properties. Here, we compare molecular mechanical (MM) fixed point charges to a polarizable continuum model (PCM) for computing electronic excitations in solution. We computed the excitation energy of three pairs of neutral/anionic molecules in aqueous solvent, including up to 250 water molecules in the QM region. Interestingly, the convergence is similar for MM point charges and a PCM, with convergence achieved when at least one full solvation shell is treated with QM. Although the van der Waals (VDW) definition of the PCM cavity is adequate with small amounts of QM solvent, larger QM solvent layers had gaps in the VDW PCM cavity, leading to asymptotically incorrect excitation energies. Given that the VDW cavity leads to unphysical solute–solvent interactions, we advise using a solvent-excluded surface cavity for QM/PCM calculations that include QM solvent.



INTRODUCTION

Excited states of chromophores play a key role in charge-transfer and energy-conversion processes. These chemical processes typically occur in the condensed phase and the surrounding environment can have a significant effect on the absorption and emission spectra of chromophores.^{1,2} The electrostatic potential of the environment and its polarization can stabilize the ground and excited states of the chromophore and participate in charge and proton transfer with the solute. There are various models that attempt to account for the interactions between the chromophore and its environment. One approach is to describe the environment with quantum mechanics (QM), but this becomes computationally intractable for systems larger than a few hundred atoms. A more computationally feasible approach is to treat the chromophore with QM and the surrounding environment with a classical model, such as molecular mechanical (MM) point charges (the QM/MM method)^{3–6} or a polarizable continuum model (PCM).^{7–10} This hybrid QM/classical approach has proven effective in modeling enzyme catalysis^{11–16} and electronic excitations of chromophores in both solution^{17–22} and protein environments.^{23–26} When modeling ionization, including the effects of solvent polarization is essential for obtaining correct energies;²⁷ for ionization processes, a point charge MM model of the solvent will fail, and a method that captures long-range polarization is essential. However, it is not clear if the same polarization requirement is essential for modeling molecular excitations. Here, we focus on the effects of

the QM/MM model compared to the QM/PCM model on electronic transitions of chromophores in solution.

Using standard nonpolarizable MM force fields, the QM/MM method embeds the QM nuclear charges and QM electron density in a field of static point charges representative of the solvent. The static MM point charges polarize the QM electron density, but the MM point charges remain unchanged throughout the ground- and excited-state calculation. With the QM/PCM method, the QM charge density is enclosed in a cavity surrounded by a dielectric continuum, and the response of the dielectric to the QM charge density evaluated at the cavity surface is included in the effective Hamiltonian. Thus, both classical solvent models include polarization of the QM region, but only QM/PCM includes the mutual polarization of the solvent and QM charge density. This polarization may model solute–solvent interactions more accurately than the static point charges of standard MM force fields, but the dielectric continuum does not include site-to-site interactions, such as hydrogen bonding. These interactions can be modeled with MM point charges. Perhaps the best QM/classical model includes the polarizability of the MM point charges in response to the QM density. Several polarizable MM force fields have been developed using a variety of models, such as induced dipoles,^{28–30} fluctuating charges,³¹ and Drude oscillators,³² but because these methods are not

Received: September 10, 2016

Revised: October 26, 2016

Published: October 31, 2016

widely available in standard software packages, they will not be explored in this work.

Instead of treating only the solute with QM, the description of the solute–solvent interaction can be improved by including some of the solvent in the QM region. When using both QM and classical solvent, one must determine how much solvent should be treated with QM. In addition, it is unclear whether the specific interactions of MM charges or the polarizable response of a PCM is more accurate when interfacing with a QM solvent. This is the question we turn to in this work.

For modeling the excitation energies of chromophores in solution using large amounts of explicit QM solvent, we will need a method that is computationally affordable enough to take into account hundreds of QM solvent molecules. In this work, we use linear response time-dependent density-functional theory (TDDFT) because it provides a good balance of computational affordability and accuracy.^{33,34} However, TDDFT has known charge-transfer errors,^{33,35,36} especially when computing excitation energies of chromophores in solution.^{37–39} For these systems, charge-transfer transitions between solvent molecules at the exterior of the solvent shell and the chromophore occur at spuriously low energies that are at or below the energies of valence transitions of the chromophore.⁴⁰ This charge-transfer error is predominantly due to the lack of the correct Coulombic interaction potential between the electron and hole in approximate xc functionals. Using a long-range corrected hybrid functional^{41–43} that includes 100% exact exchange at long range with a classical bulk environment will correct the energy of the solvent–solute charge-transfer transitions, separating them from the low-energy valence excitations of the chromophore.⁴⁴ We therefore use this procedure for all of our TDDFT calculations.

With large amounts of explicit QM solvent, the QM/classical model approaches the limit of full QM treatment of the solute–solvent system, and excitation energies are expected to converge. This convergence with respect to the size of the QM region has been previously studied using QM/MM^{18,22,45–47} and QM/PCM^{44,48–50} models. In some cases, convergence was obtained with only a few QM solvent molecules, whereas hundreds of QM solvent molecules were required in others. For example, the vertical excitation energy of aqueous acetone converged with six or fewer QM water molecules using QM/PCM⁴⁸ and QM/MM,^{22,45} and the QM/MM excitation energy of aqueous acrolein converged with just two QM water molecules.⁴⁶ These studies suggest that excitation energies of the relatively small molecules of acetone (10 atoms) and acrolein (7 atoms) converge with QM treatment of only the hydrogen-bonded water molecules. The absorption maximum of bacteriochlorophyll *a* (~80 atoms) was computed in aqueous solvent using the semiempirical QM method ZINDO/S-CIS (Zerner intermediate neglect of differential orbital method with the configuration interaction method using only single excitations) and found to converge with about 40 water molecules.⁴⁷ The absorption maximum of aqueous *N,N*-diethyl-4-nitroaniline (28 atoms) was predicted by TD-B3LYP/PCM to converge with about 20 QM water molecules.⁴⁴ Although these studies suggest that more than hydrogen-bonded QM water molecules are necessary to converge QM/classical excitation energies, convergence was achieved with fewer than the number of water molecules in the first solvation shell of the chromophore. In contrast, the ZINDO/S-CIS spectra of phenol blue (31 atoms) indicate that more than 150 QM water molecules are required to reach convergence of the excitation energy to within 0.10 eV.¹⁸ Alizarin (26 atoms), a chromophore of similar size as

phenol blue, required about 150 QM water molecules to achieve convergence of the solvatochromic shift to within 0.05 eV using TD-PBE/PCM.⁵⁰ In summary, some studies suggest that a relatively large amount of QM solvent is necessary to converge QM/classical excitation energies, whereas others report convergence with only hydrogen-bonded water molecules treated with QM, and yet others report that an intermediate amount of explicit solvent is necessary. In most of these studies, only a single solute was examined. In this article, we compare results for six solutes of different sizes and polarities.

To our knowledge, only a couple of studies have compared QM/MM and QM/PCM excitation energies of aqueous chromophores.^{49,50} In these studies, explicit QM water molecules were replaced by QM-derived atomic point charges (computed using the QM/PCM model) or TIP3P point charges, a standard 3-point water model. QM/classical excitation energies were compared using QM/PCM with no QM solvent, QM/PCM with QM solvent, and QM/MM/PCM with no QM solvent. One study suggests that site-specific electrostatic solute–solvent interactions from QM/MM/PCM calculations are sufficient to reproduce QM/PCM excitation energies with hydrogen-bonded QM water molecules.⁴⁹ The other study reports mixed results, largely dependent on the solute–solvent configuration, when a large number (about one solvation shell) of QM water molecules are replaced by QM-derived point charges or TIP3P point charges.⁵⁰ To the best of our knowledge, the work presented herein is the first study to directly compare the convergence of QM/MM and QM/PCM excitation energies with respect to a systematic increase in the number of QM water molecules.

We do not necessarily expect the QM/MM and QM/PCM excitation energies to agree for small amounts of explicit QM solvent due to differences in the QM/MM and QM/PCM models. However, we expect the QM/MM and QM/PCM TDDFT excitation energies to agree in the limit of large amounts of QM solvent because the QM solvent will screen the localized excitation on the chromophore from the classical environment (MM or PCM) and account for the fast solvent polarization upon excitation. The question we aim to answer is whether the specific atomistic interactions of MM point charges or the mutual polarization of the PCM method will lead to convergence of QM/classical excitation energies with fewer QM solvent molecules.

To address this question, we compare the convergence of QM/MM and QM/PCM excitation energies with respect to the size of the QM solvent region for three neutral/anion pairs of increasing molecular size in aqueous solution: phenol and phenolate, *trans*-thiophenyl-*p*-coumarin and coumarate (*p*C^T and *p*C^{T−}, which are neutral and anionic analogues of the photoactive yellow protein chromophore), and neutral and anionic fluorescein (see molecules in Figure 1). The excited states examined for *p*C^{T−} and the fluorescein anion have substantial charge-transfer character, with electron density going from the negatively charged oxygen site to the antibonding π system. After a brief review of QM/classical theory and the implementation of TDDFT within QM/classical methods, we discuss the effects of the definition of the PCM cavity and the MM point charge values on the convergence of QM/classical excitation energies using *p*C^{T−} as an example. The convergence of QM/MM and QM/PCM excitation energies is then directly compared for all six solutes. The article concludes with general guidelines for the amount of explicit solvent necessary to achieve convergence of QM/classical excitation energies.

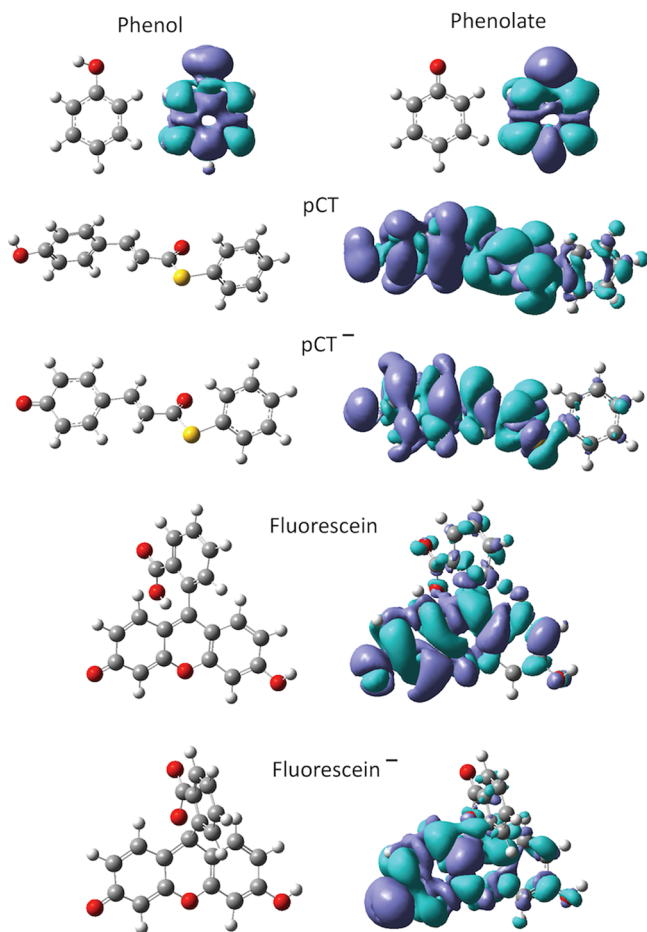


Figure 1. Structures and ground–excited state density difference plots for each solute. The gray atoms represent carbons, the red atoms are oxygens, the yellow is sulfur, and the white atoms are hydrogens. The blue and purple isosurfaces (isovalue = 0.0004) represent increase and decrease in electron density in the excited state relative to the ground-state electron density, respectively.

THEORY

QM/Classical Solvent Models. MM force fields^{6,12} use classical potential energy functions to model bonded (bond stretching, angle bending, and dihedral torsions) and nonbonded (Coulombic and van der Waals (VDW)) interactions between MM atoms. The most common approach to modeling the Coulombic interaction of QM and MM atoms is electrostatic embedding, where MM point charges interact with the QM electron density through the one-electron term and the fixed QM nuclei through a point charge term. The QM/MM portion of the Hamiltonian is

$$\hat{H}_{\text{QM/MM}} = \sum_{A \in \text{MM}} \int \frac{Q_A}{|\mathbf{r} - \mathbf{R}_A|} d\mathbf{r} + \sum_{A \in \text{MM}} \sum_{B \in \text{QM}} \frac{Z_B Q_A}{|\mathbf{R}_B - \mathbf{R}_A|} \quad (1)$$

where \mathbf{r} is the electronic coordinate, Q_A is an MM point charge at position \mathbf{R}_A , and Z_B is a QM nuclear charge at position \mathbf{R}_B . QM/MM methods efficiently model long-range electrostatic effects and specific atomistic electrostatic interactions, thus taking into account some of the energetics of hydrogen bonding. However, standard MM force fields use fixed point charges and do not

include polarization of the MM region with respect to the QM region. The classical MM point charges that surround the QM solvent and solute can provide electrostatic stabilization of the QM subsystem and hydrogen bonding directly through the QM/MM boundary.

There are a variety of continuum models,^{9,10} but the most common ones use apparent surface charges. In this approach, the charge density of the QM region is enclosed in a cavity surrounded by a dielectric continuum. The response of the dielectric to the QM charge density is included in the QM Hamiltonian as an apparent surface charge evaluated at the cavity surface (Γ)

$$\hat{H}_{\text{QM/PCM}} = \int_{\Gamma} \phi[\rho](\mathbf{s}) \sigma[\epsilon, \rho](\mathbf{s}) d\mathbf{s} \quad (2)$$

Here, $\phi[\rho](\mathbf{s})$ is the electrostatic potential due to the QM electron density and the nuclei evaluated at position \mathbf{s} on the cavity surface

$$\phi[\rho](\mathbf{s}) = \int \frac{1}{|\mathbf{r} - \mathbf{s}|} d\mathbf{r} + \sum_{B \in \text{QM}} \frac{Z_B}{|\mathbf{R}_B - \mathbf{s}|} \quad (3)$$

where \mathbf{r} is the electronic coordinate and Z_B is a QM nuclear charge at position \mathbf{R}_B . In eq 2, $\sigma[\epsilon, \rho]$ is the apparent surface charge density

$$\sigma[\epsilon, \rho](\mathbf{s}) = \int_{\Gamma} V_R[\epsilon, \rho](\mathbf{s}) \phi[\rho](\mathbf{s}') d\mathbf{s}' \quad (4)$$

where $V_R[\epsilon, \rho]$ is the solvent response function dependent on the solvent dielectric constant (ϵ) that may be separated into fast (ϵ_{∞}) and slow (ϵ_s) components. Alternative formulations define the dielectric constant outside of the cavity as infinite ($\epsilon = \infty$) and are known as conductor-like screening models.^{51–56} The resulting apparent surface charge density is then scaled by a factor dependent on the realistic dielectric constant of the solvent. In each of these polarizable continuum methods, the solvent response function ($V_R[\epsilon, \rho]$) captures the polarization of the bulk dielectric due to the QM electron density evaluated at the cavity surface. Because $V_R[\epsilon, \rho]$ is dependent on the shape of the cavity, it is not uniquely defined. In fact, many approaches have been proposed to define the shape of the molecular cavity. The simplest approach uses a sphere or ellipsoid of appropriate size to define the cavity, but this definition neglects molecular specificity. The most common approach is to define the surface in terms of overlapping spheres centered on the QM nuclei, where the size of each sphere is defined by the VDW radii of the QM nuclei. This surface is referred to as the VDW surface and is often the default in electronic structure programs, such as Gaussian09.⁵⁷ Different sets of VDW radii are available, including the universal force field⁵⁸ and those of the SMD solvation model.⁵⁹ The VDW surface neglects the physical constraints of the size of the solvent molecules. Alternative definitions of the cavity surface use a solvent probe of appropriate size to define the solvent-excluded surface (SES) or the solvent-accessible surface.^{60,61} An isosurface of the total QM electron density^{62,63} or QM charge density⁶⁴ can also be used to define the cavity surface. In practice, the cavity surface is divided into elements called tesserae, and point charges are defined at the center of each tessera (\mathbf{s}_k)

$$q_k[\epsilon, \rho](\mathbf{s}_k) = a_k \sigma[\epsilon, \rho](\mathbf{s}_k) \quad (5)$$

where a_k is the area of tessera k and $\sigma[\epsilon, \rho](\mathbf{s}_k)$ is the apparent surface charge density within that tessera. These apparent surface

Table 1. Summary of QM/MM Electronic Transitions Analyzed for Each Solute^a

	transition ^b	energy separation (eV)	MO character	excitation energy (eV)	oscillator strength
phenol	S ₁	~1.0	HOMO → LUMO	5.3–5.7	0.02–0.05
phenolate	S ₁	~1.0	HOMO → LUMO	4.8–5.1	0.10–0.11
pCT	S ₂	0.1–0.4	HOMO → LUMO or HOMO – 1 → LUMO	4.8–5.3	0.05–1.30
pCT ⁻	S ₁	~1.0	HOMO → LUMO	3.5–3.8	1.20–1.40
fluorescein	S ₁	0.1–0.3	HOMO → LUMO	3.2–3.5	0.45–0.50
fluorescein ⁻	S ₂	0.2–0.5	HOMO → LUMO + n	4.7–5.0	0.05–0.12

^aAll water molecules treated with MM. ^bThe lowest energy and second lowest energy transitions are labeled S₁ and S₂, respectively.

charges define the electrostatic response of the solvent at each point on the cavity surface. The QM/PCM interaction term of the Hamiltonian is then a sum over point charges

$$\hat{H}_{\text{QM/PCM}} = \sum_k \phi[\rho](\mathbf{s}_k) q_k [\epsilon, \rho](\mathbf{s}_k) \quad (6)$$

where $\phi[\rho]$ is evaluated at point \mathbf{s}_k on the cavity surface. Within the self-consistent field procedure, the QM/PCM interaction potential due to $\hat{H}_{\text{QM/PCM}}$ is computed iteratively in a self-consistent manner, that is, a self-consistent reaction field (SCRF) method, and mutual polarization between the QM and MM regions is achieved.

TDDFT/Classical Excitation Energies. As with ground-state DFT, TDDFT is formally exact, but in practice the excitation energies are approximated due to the unknown form of the exchange-correlation (xc) functional, f^{xc} .^{33,34} The linear response TDDFT excitation energies are computed by solving for the eigenvalues of the linear response matrix^{65,66}

$$\begin{bmatrix} \mathbf{A} & \mathbf{B} \\ \mathbf{B}^* & \mathbf{A}^* \end{bmatrix} \begin{bmatrix} \mathbf{X} \\ \mathbf{Y} \end{bmatrix} = \omega \begin{bmatrix} 1 & 0 \\ 0 & -1 \end{bmatrix} \begin{bmatrix} \mathbf{X} \\ \mathbf{Y} \end{bmatrix} \quad (7)$$

where ω are the excitation energies, and X and Y are the corresponding transition density vectors. The oscillator strength of each transition is defined as

$$f_i = \frac{2}{3} \omega_i \sum_{k=x,y,z} |\mu_{ik}|^2 \quad (8)$$

where μ_{ik} is the one-dimensional transition dipole moment computed for eigenvectors X_i and Y_i . The A and B matrix elements are defined as

$$A_{ai,bj} = \delta_{ab} \delta_{ij} (\epsilon_a - \epsilon_i) + \langle i a | b j \rangle + f_{ai,bj}^{\text{xc}} \quad (9)$$

$$B_{ai,bj} = \langle i a | b j \rangle + f_{ai,bj}^{\text{xc}} \quad (10)$$

where ϵ_i and ϵ_a are the ground-state molecular orbital (MO) energies of the occupied and virtual MOs, respectively, and $\langle i a | b j \rangle$ and $f_{ai,bj}^{\text{xc}}$ are the two-electron integrals resulting from terms in the Kohn-Sham matrix that depend on the electron density, namely, the Coulomb and xc terms, respectively. Because the MM point charges in the QM/MM Hamiltonian do not depend on the electron density, these charges do not directly show up in the TDDFT response equations and only affect the excitation energies indirectly through the ground-state determination of the MOs and their energies. For linear response TDDFT PCM calculations,¹⁰ the A and B matrix elements include an additional term, $V_{ai,bj}^{\text{PCM}}$, that takes into account the fast dielectric response of the solvent during a vertical excitation

$$A_{ai,bj} = \delta_{ab} \delta_{ij} (\epsilon_a - \epsilon_i) + \langle i a | b j \rangle + f_{ai,bj}^{\text{xc}} + V_{ai,bj}^{\text{PCM}} \quad (11)$$

$$B_{ai,bj} = \langle i a | b j \rangle + f_{ai,bj}^{\text{xc}} + V_{ai,bj}^{\text{PCM}} \quad (12)$$

where

$$V_{ai,bj}^{\text{PCM}} = \sum_k \left(\int \psi_a^* \psi_i \frac{1}{|\mathbf{r} - \mathbf{s}_k|} d\mathbf{r} \right) q_k [\epsilon_{\infty}, \psi_b^* \psi_j](\mathbf{s}_k) \quad (13)$$

In this term, the QM electrostatic potential due to electron density $\psi_a^* \psi_i$ is evaluated at point \mathbf{s}_k on the cavity surface, and the apparent surface point charge (q_k) is derived from the fast component of the solvent dielectric (ϵ_{∞}) in response to the QM electron density $\psi_b^* \psi_j$ at the same point on the cavity surface.^{67,68} Therefore, the polarizable environment of the QM/PCM model affects the excitation energy both directly through the $V_{ai,bj}^{\text{PCM}}$ term in the TDDFT equations and indirectly through the ground-state determination of the MOs and their energies, whereas the fixed point charges of the QM/MM model affect the excitation energy only indirectly through the MOs.

COMPUTATIONAL DETAILS

Molecular Dynamics and Solvation Shells. The solute–solvent configurations were obtained from snapshots of classical molecular dynamics simulations performed in AMBER 12.⁶⁹ The purpose of these simulations was not to ensure the most accurate excitation energies, but to sample solute–solvent configurations. The Antechamber program (an AMBER accessory module) was used to assign solute atom types and charges, whereas force field parameters were obtained from the general AMBER force field.^{70,71} The solute was then solvated with a pre-equilibrated 32 Å sphere of TIP3P waters⁷² that included over 4000 water molecules. Periodic boundary conditions were not used, and all electrostatic terms were included. After energy minimization and equilibration to room temperature and pressure, snapshots of the molecular coordinates were saved in intervals of 500 fs. Five snapshots from each set of dynamics are analyzed here.

Because the solutes are nonspherical, radial distribution functions were not found useful in determining the number of water molecules needed to complete the first and second solvation shells of each solute. Instead, we counted the number of water molecules within a given distance of any atom of the solute and identified breaks in the linearity of this function that correspond to differentiation of solvation shells. Using this approach, the number of water molecules in the first solvation shell was found to be approximately 30–35 for phenol and phenolate, 96–111 for pCT and pCT⁻, and 118–128 for fluorescein and its anion. For our QM/MM convergence studies, we use up to 250 water molecules in the QM region. For phenol and phenolate, this corresponds to the most distant solvent being 11 Å away from any atom in the solute, whereas for pCT, pCT⁻, fluorescein, and the fluorescein anion, the most distant solvent molecules are 9 Å away from any atom in the solute. The distance corresponding to the first solvation shell is about 5 Å for phenol

and phenolate, 6 Å for pCT and pCT⁻, and 7 Å for fluorescein and its anion.

QM/Classical Calculations. A combined QM/classical approach was used to compute excitation energies, where the QM region was treated with linear response TDDFT within the Tamm–Dancoff approximation.⁷³ The Gaussian09 electronic structure program⁵⁷ was used for all QM/MM and QM/PCM TDDFT calculations. The five lowest energy transitions were computed for each solute. The number of explicit water molecules treated with QM was increased from zero (i.e., the solute-only QM region) to 250. At each QM region size, the transition with the largest oscillator strength was analyzed, with a few exceptions where transitions of similar MO character were analyzed (Table 1). The implicit solvent was modeled by the integral equation formalism of PCM (IEF-PCM),^{10,74,75} which is the default SCRF method in Gaussian09, with the default dielectric constants for water ($\epsilon_s = 78.355300$, $\epsilon_\infty = 1.777849$). For QM/MM calculations where only the solute is treated with QM, all the point charges from the molecular dynamics were included via nonpolarizable electrostatic embedding. For calculations with QM solvent, the closest water molecules to any atom of the solute were converted from MM to QM and included in the QM region. For QM/MM, all remaining water molecules were included as MM fixed point charges. For QM/PCM calculations, the QM region was enclosed in a cavity defined by overlapping spheres. The radii of the spheres used to define the PCM cavity can affect the accuracy and convergence of excitation energy calculations.^{44,48} In this work, the surface of the cavity was either a VDW surface derived from universal force field atomic radii scaled by 1.1 (Gaussian09 default) or from universal SES.

Additional analysis in this work uses the CHELPG procedure,⁷⁶ in which atomic point charges of QM water molecules were derived from the QM electrostatic potential of QM/classical calculations with explicit solvent. These QM-derived point charges were then used as input for QM/MM calculations or to quantify the amount of charge transfer to water molecules using QM/MM and QM/PCM. For CHELPG charges of the excited state, we used the excited-state density obtained from a state-specific approach (Gaussian keywords TD(root = X), density = current, and population = CHELPG).

Density Functionals and Basis Sets. In this work, we use the long-range corrected functional ω B97X;⁷⁷ by default, this functional includes about 16% exact exchange at short range and 100% at long range and has a range-separation parameter of 0.3 bohr⁻¹. Because of the charge-transfer error, global hybrids with a large percentage of exact exchange (over 50%) or long-range corrected hybrids are recommended for TDDFT calculations that include QM water molecules. To compare how convergence of excitation energy varies across functionals with different amounts of exact exchange, calculations were also performed with M06-2X,⁷⁸ a global hybrid functional with 54% exact exchange; M06-HF,⁷⁹ a global hybrid functional with 100% exact exchange; LC- ω PBE,⁸⁰ a long-range corrected functional with a range-separation parameter of 0.2 bohr⁻¹; and ω B97XD,⁸¹ the ω B97X functional with Grimme's empirical dispersion correction,⁸² with about 22% exact exchange at short range and a range-separation parameter of 0.2 bohr⁻¹. The bright-state excitation energies of a single snapshot of pCT⁻ using the 6-31G(d) basis set are shown in Figure S1. Although the excitation energy of each functional converges to a different value, there is similar convergence of excitation energies with respect to the size of the QM region for these hybrid functionals that include a large

amount of exact exchange. Although convergence trends are likely to vary between snapshots, the results shown in Figure S1 suggest that the functionals tested here would behave similarly.

Due to the number of QM/classical calculations in this study with large amounts of QM solvent, moderate basis sets are used. Calculations on pCT and pCT⁻ use the 6-31G(d) basis set, and the 6-31G basis set is used for phenol and phenolate and neutral and anionic fluorescein. To examine the effect of the size of the basis set on the convergence of QM/classical excitation energies, the TDDFT QM/MM excitation energy of a single snapshot of pCT⁻ was computed using the 6-31G, 6-31G(d), and 6-31+G(d) basis sets with increasing number of QM waters (Figure S1). Adding a *d* function to polarize the *p* functions of the 6-31G basis set reduces the converged excitation energy by 0.37 eV, and adding a diffuse function to the 6-31G(d) basis set reduces the converged value by an additional 0.06 eV. Although the converged values differ as the basis set increases, the convergence of the excitation energy is similar for the three basis sets considered here.

RESULTS AND DISCUSSION

Electrostatic embedding QM/MM methods capture the electronic polarization of the QM region by the classical MM fixed point charges and include specific hydrogen-bonding interactions, but they do not include polarization of the MM environment in response to the QM electron density. A classical PCM includes mutual polarization between the QM region and the classical environment but is missing the specific atomistic interactions. For the PCM, the QM region is enclosed in a cavity and surrounded by a dielectric continuum, which is defined by a dielectric constant that is a measure of the polarizability of the solvent. Given a large enough layer of QM solvent surrounding the localized excitation on the solute, the polarization is taken into account by the nearest QM water molecules and we expect the excitation energies to converge to the same value regardless of the classical model. This is because when the classical region is sufficiently removed from the solute and screened by the QM water molecules, the solute-classical interactions should be dominated by long-range electrostatics that are taken into account by both MM point charges and the PCM.

MM Point Charges with QM Solvent. To test the effect of the magnitude of MM point charges on the convergence of QM/MM excitation energies, we computed excitation energies of pCT⁻ using TIP3P point charges⁷² (oxygen = -0.8340e, hydrogen = 0.4170e), SPC/E point charges⁸³ (oxygen = -0.8476e, hydrogen = 0.4238e), halved TIP3P point charges (oxygen = -0.4170e, hydrogen = 0.2085e), and doubled TIP3P point charges (oxygen = -1.6680e, hydrogen = 0.8340e). Scaling the value of the point charges will change the electric field generated by the MM charges, affecting the electronic structure of the solute and the resulting excitation energy. Because the dipole moment of the point charge waters has changed, there is likely a larger discrepancy between the QM solvent and the MM point charge solvent at the QM/MM interface.

To test how this disparity at the QM/MM interface affects the convergence of the excitation energies, we show results for a single snapshot of pCT⁻ in Figure 2. The QM/MM excitation energies computed with TIP3P point charges and SPC/E point charges agree within 0.01 eV for all amounts of explicit solvent. When the magnitudes of the TIP3P MM point charges are doubled or halved, the QM/MM excitation energies are noticeably different from those computed with standard TIP3P point charges. For example, the QM/MM excitation energies

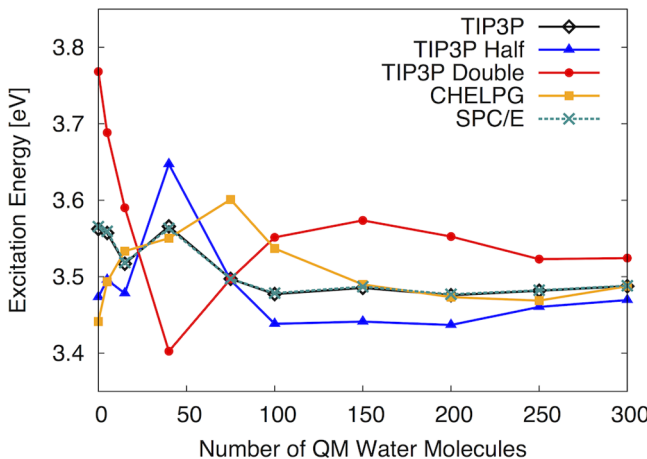


Figure 2. TDDFT excitation energies of a single snapshot of pCT^- computed using the 6-31G(d) basis set and the ωB97X functional in a QM/classical approach, where the classical region is modeled with TIP3P point charges (TIP3P), SPC/E point charges (SPC/E), half the value of TIP3P point charges (TIP3P Half), double the value of TIP3P point charges (TIP3P Double), and point charges derived from CHELPG analysis of 300 QM water molecules surrounded by ~ 4000 classical water molecules represented by TIP3P point charges (CHELPG). Note that the CHELPG results only extend to 300 QM water molecules.

computed for one snapshot of pCT^- using MM point charges that are half (double) the value of TIP3P point charges differ by up to 0.09 eV (0.21 eV) from values computed with TIP3P point charges. For the five snapshots analyzed, with 400 QM water molecules, the halved and doubled TIP3P point charges lead to a QM/MM excitation energy with different values compared to TIP3P point charges (Table S1); the halved TIP3P point charges underestimate the QM/MM excitation energy by an average of 0.04 eV, whereas the doubled TIP3P point charges overestimate the excitation energy by an average of 0.08 eV relative to the TIP3P point charges. In terms of convergence, both doubled and halved TIP3P point charges perform worse than the TIP3P values. For all snapshots, the MM point charges with half (double) the value of TIP3P point charges require, on average, 150 (200) QM water molecules to converge the QM/MM excitation energy within 0.05 eV of the values computed with 400 QM water molecules, whereas TIP3P point charges require, on average, only 75 QM water molecules (convergence results for all snapshots are given in Figure S2).

To investigate whether the excitation energy convergence could be improved by using charges derived from the QM electron density, we computed QM/MM excitation energies using fixed MM point charges, where up to 300 of the nearest MM water molecules are replaced by atomic point charges derived from CHELPG⁷⁶ analysis of a QM/MM calculation with 300 QM water molecules embedded in TIP3P MM point charges. This approach takes into account some polarization of the classical solvent by the QM electron density, as the water point charges now vary considerably depending on the orientations of the water molecules within the solute–solvent configuration: the oxygen charge ranges from $-0.34e$ to $-1.39e$ with an average value of $-0.86e$, and the hydrogen charge ranges from $0.16e$ to $0.78e$ with an average value of $0.43e$. The QM/MM excitation energy of a single snapshot of pCT^- computed with CHELPG point charges is shown in Figure 2. With 250 QM water molecules, the CHELPG MM point charges give an

excitation energy within 0.01 eV of the value computed with TIP3P point charges. However, the CHELPG excitation energies of the other snapshots differ up to 0.04 eV from the TIP3P values computed with 250 QM water molecules. For all snapshots of pCT^- , QM/MM excitation energies computed with CHELPG point charges require, on average, 150 QM water molecules to be converged within 0.05 eV of the values computed with 250 QM water molecules, whereas TIP3P point charges require, on average, 75 QM water molecules (Figure S2). This slower convergence of QM/MM excitation energies with CHELPG point charges is likely due to the water point charges no longer being net neutral. Although the system has the correct total charge in the original QM/MM calculation with 300 QM water molecules, using only some of the water molecules for subsequent TDDFT QM/MM calculations means that the sum of charges on all waters is not zero, leading to long-range Coulombic interactions between the non-neutral waters and the solute that affect the excitation energy. Thus, TIP3P (or SPC/E) point charges offer better convergence of QM/MM excitation energies with respect to the QM region size compared to QM-derived CHELPG point charges. Therefore, TIP3P charges are used in the rest of this work to compute QM/MM excitation energies.

PCM Cavity with QM Solvent. To test the effect of the PCM cavity on the convergence of QM/PCM excitation energies, we computed the excitation energy of pCT^- using the IEF-PCM method with both a VDW cavity and an SES cavity. The convergence of these QM/PCM excitation energies is shown in Figure 3, along with the QM/MM excitation energy of

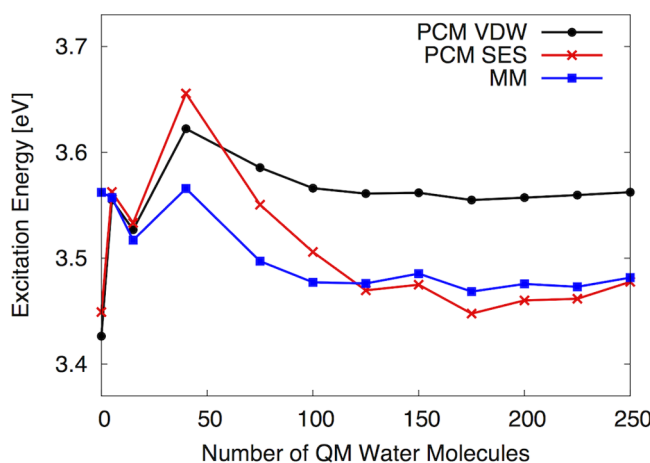


Figure 3. TDDFT excitation energies of a single snapshot of pCT^- in water computed using the 6-31G(d) basis set and the ωB97X functional in a QM/classical approach, where the classical region is modeled with TIP3P point charges (MM), PCM with a cavity defined by a VDW surface (PCM VDW), or PCM with a cavity defined by an SES (PCM SES).

the same snapshot of pCT^- computed with TIP3P point charges. For small amounts of QM solvent (5–15 QM water molecules), the VDW definition of the PCM cavity gives excitation energies that are similar to QM/MM values. However, the QM/PCM VDW and QM/MM excitation energies converge to different values, with the QM/PCM VDW excitation energy being 0.08 eV higher in energy. For the 5 snapshots, QM/PCM with a VDW cavity consistently overestimates excitation energies relative to QM/MM values computed with 250 QM solvent molecules, similar to the overpolarization seen with the larger magnitude

point charges. The maximum difference between the QM/PCM VDW and QM/MM excitation energies with 250 QM solvent molecules is 0.13 eV, with an average deviation of 0.06 eV.

The solute-only VDW cavity surface is composed of overlapping spheres with origins at the nuclei of solute atoms, see Figure 4a. As explicit solvent is added, the VDW surface is

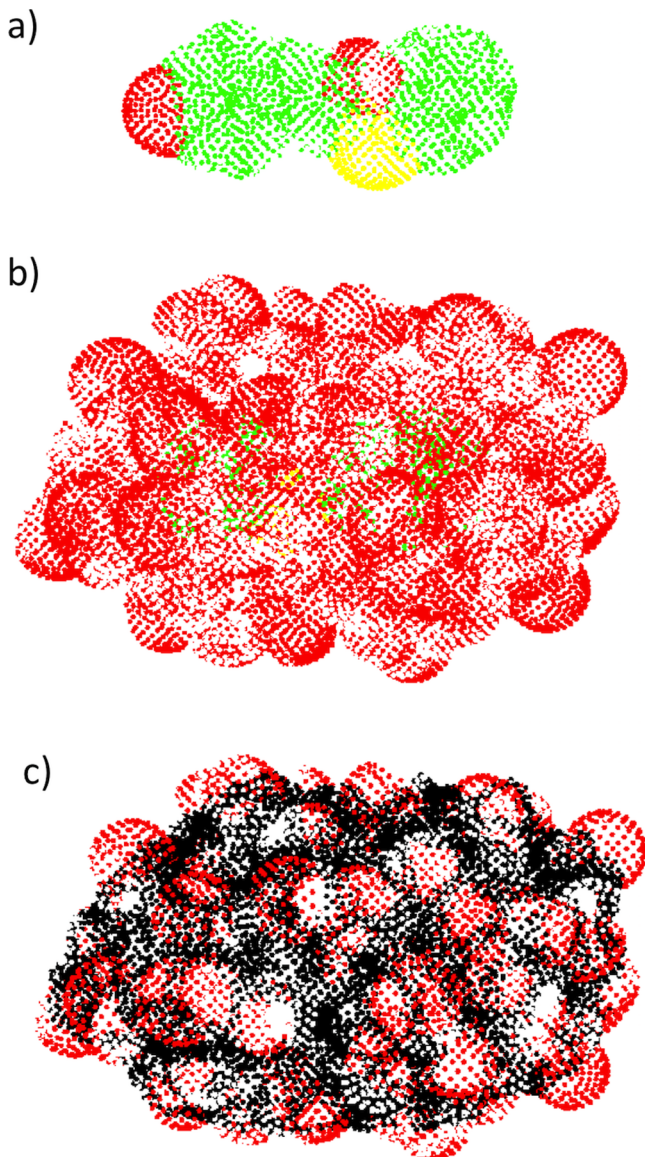


Figure 4. Tesserae of the PCM cavity surface of pCT^- computed using (a) VDW surface without QM solvent, (b) VDW surface with QM solvent, and (c) SES with QM solvent. Color indicates the atomic nuclei at the origin of the sphere on which the tessera is located: carbon (green), oxygen (red), sulfur (yellow), hydrogen (white), and added sphere (black).

additionally composed of spheres from the nuclei of water molecules, but retains some green and yellow tesserae from VDW spheres with origins at the solute nuclei (Figure 4b). Because these tesserae are located within the explicit solvent layer, where QM water molecules are already present, the VDW PCM cavity has areas in the interior of the cavity, where solvent polarization is included through the response of the dielectric and the QM treatment of explicit water molecules. This double counting of solvent polarization within the VDW cavity causes a

nonphysical overpolarization of the QM charge density and, consequently, nonphysical excitation energies that do not agree with the converged QM/MM excitation energies at the asymptotic limit.

To remedy this problem, we computed the excitation energy of pCT^- using a PCM cavity defined by an SES. This cavity uses additional spheres to “fill in” gaps left by the VDW cavity and is more suitable for calculations containing explicit QM solvent. Figure 4c shows that tesserae on the surface of the SES cavity are from VDW spheres with origins at solvent nuclei and added spheres (shown in black). The excitation energies computed with the SES cavity are shown in Figure 3. From 0 to 40 QM water molecules, the SES and VDW cavities are similar, and the QM/PCM SES and QM/PCM VDW excitation energies are also similar. Once the first solvation shell is treated with QM (75 + QM water molecules), the QM/PCM SES excitation energy diverges from the QM/PCM VDW excitation energy and aligns with the QM/MM excitation energy. With two QM solvation shells (250 QM water molecules), the QM/PCM SES and QM/MM excitation energies converge to the same value (3.48 eV), as expected. This is true for all snapshots, with an average absolute deviation of 0.01 eV between the QM/MM and QM/PCM SES excitation energies computed with 250 QM water molecules. Given that the VDW cavity leads to unphysical solute–solvent interactions, it is advised to use the SES cavity for QM/PCM calculations that include large amounts of QM solvent.

Comparison of Excitation Energy Convergence with QM/MM and QM/PCM. Using the SES cavity with PCM and TIP3P point charges with MM, we compare the convergence of excitation energies computed with PCM and MM point charge environments for five snapshots of each of the six solutes. Unlike the bright lowest energy state of pCT^- , the low-energy electronic transitions of the other solutes have relatively small oscillator strengths (Table 1). For phenol and phenolate, the lowest energy transition is well separated in energy from higher energy transitions and is always analyzed regardless of oscillator strength. However, the lowest energy transitions of pCT , fluorescein, and the fluorescein anion are within 0.5 eV of higher energy transitions and may have similar oscillator strength as these higher energy transitions. Therefore, transitions of similar character were selected for analysis, as indicated in Table 1.

In the Supporting Information (SI), we analyze the amount of charge transfer from each solute to the QM solvent upon excitation. Figure S3 shows the average amount of charge transfer for five snapshots of each solute, where the amount of charge transfer is computed as the absolute difference in the total charge of the solvent in the ground and excited states based on the CHELPG⁷⁶ atomic point charges derived from the ground- and excited-state electron densities. We found that for all solutes, the average amount of charge transfer computed with QM/MM and QM/PCM agrees within 0.005e when at least 15 QM solvent molecules are included. However, for the anionic solutes, PCM induces more charge transfer (0.005e–0.013e) than MM point charges when only the nearest five water molecules are treated with QM.

We first compare the convergence of QM/classical excitation energies for neutral solutes: phenol, pCT , and fluorescein (Figure 5). In the convergence figures, we plot the difference in excitation energy compared to the value with 250 QM water molecules. For the three neutral solutes, both QM/MM and QM/PCM tend to overestimate the excitation energy with no QM solvent relative to values computed with 250 QM water molecules. The average overestimation of the QM/MM

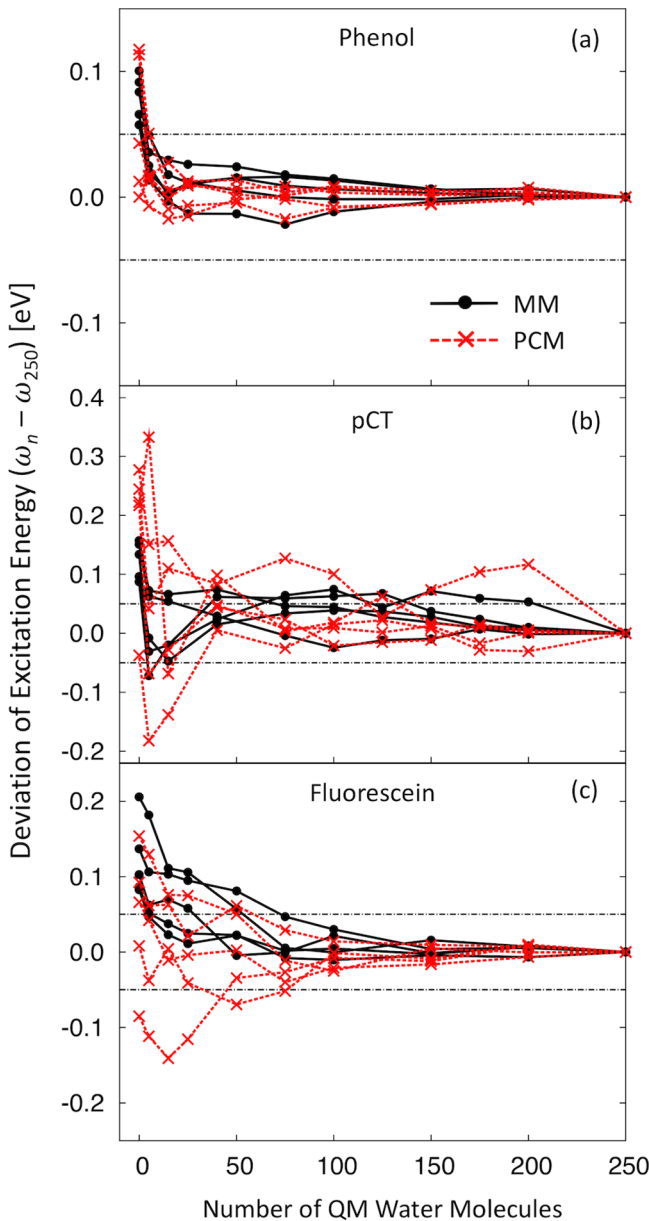


Figure 5. Deviation of QM/classical excitation energies from the values computed with 250 QM water molecules ($\omega_n - \omega_{250}$) for five snapshots of (a) phenol, (b) pCT, and (c) fluorescein. The classical region is modeled by TIP3P point charges (MM) or PCM with an SES cavity (PCM). The black dashed-dotted lines indicate deviation of ± 0.05 eV from the values computed with 250 QM water molecules.

excitation energy for phenol with no QM water molecules is 0.08 eV; this value is reduced to 0.03 eV with 5 QM water molecules. In fact, for both QM/MM and QM/PCM, all snapshots of phenol are converged to within 0.05 eV of the values computed with 250 QM water molecules when the nearest five water molecules are treated with QM, showing the best convergence of all of the solutes considered in this work. This convergence is likely due to negligible charge transfer from phenol to QM water molecules upon excitation (Figure S3). Of all the solutes studied, pCT has the worst convergence of QM/classical excitation energies with respect to the QM region size. Although the average absolute deviation in QM/MM excitation energy is significantly reduced from 0.12 to 0.05 eV as the QM region is increased from 0 to 5 QM water molecules, it remains relatively

constant as the QM region size is increased to include the first and second solvation shells. The average absolute deviation in QM/PCM excitation energies of pCT steadily decreases from 0.20 to 0.06 eV on going from 0 to 40 QM water molecules, but remains relatively constant with larger amounts of QM solvent. Thus, QM/MM excitation energies of pCT have better convergence than QM/PCM for QM regions that partially complete the first solvation shell (5 to 40 QM water molecules), but both models require large amounts of QM solvent to converge the excitation energies of all five snapshots of pCT to within 0.05 eV. This slow convergence is likely due to significant charge transfer from pCT to QM solvent (Figure S3) and large deviations in the TDDFT eigenvectors, as quantified by the transition dipole moment (Figure S4). For the largest neutral molecule, fluorescein, the QM/MM and QM/PCM excitation energies have similar convergence. The average absolute deviation in QM/MM excitation energies of fluorescein steadily decreases from 0.09 eV with 5 QM water molecules to 0.01 eV with 75 QM water molecules, at which point the excitation energies of all snapshots are within 0.05 eV of the converged values. The average absolute deviation in QM/PCM excitation energies of fluorescein decreases from 0.08 to 0.03 eV as the QM region increases from 5 to 75 QM water molecules. Thus, both QM/MM and QM/PCM excitation energies of fluorescein are converged within 0.05 eV with 75 QM water molecules, but the QM/PCM excitation energies deviate from the converged values to a greater extent than QM/MM excitation energies.

The convergence results showing the deviation in the excitation energy compared to the value with 250 QM water molecules for the anionic solutes are shown in Figure 6. Phenolate and the fluorescein anion show very similar convergence, so the trends for these solutes are discussed together. Both QM/MM and QM/PCM underestimate the excitation energy with no QM solvent, with the underestimation being significantly larger for QM/PCM. For solute-only QM regions, the QM/MM excitation energies are underestimated by an average of 0.10 eV for phenolate and 0.15 eV for the fluorescein anion. These values are reduced to 0.05 and 0.02 eV, respectively, when the nearest five water molecules are included in the QM region. With no QM solvent, the average absolute deviation in the QM/PCM excitation energy is 0.43 eV for phenolate and 0.36 eV for the fluorescein anion; this is reduced to 0.07 and 0.05 eV, respectively, when the nearest five water molecules are treated with QM. Thus, even when charge transfer and site-specific polarization are accounted for by treating the hydrogen-bonded waters with QM, modeling the remainder of the solvent as a bulk dielectric results in a larger deviation in excitation energy than the use of MM point charges for these anionic solutes.

For the pCT⁻ solute with no QM water molecules, QM/MM overestimates the excitation energy relative to the values computed with 250 QM water molecules with an average absolute deviation of 0.15 eV. For partial completion of the first solvation shell, this deviation decreases from 0.10 to 0.02 eV, as the number of QM water molecules increases from 5 to 100. With 125 QM water molecules, the QM/MM excitation energies of all five snapshots of pCT⁻ converge to within 0.05 eV of the value computed with 250 QM water molecules. This convergence is similar to the convergence of QM/MM excitation energies of alizarin that require relatively large amounts of explicit solvent due to the delocalization of the transition density onto QM water molecules within 7 Å of the solute.⁵⁰ With no QM water molecules, the QM/PCM excitation energies of pCT⁻

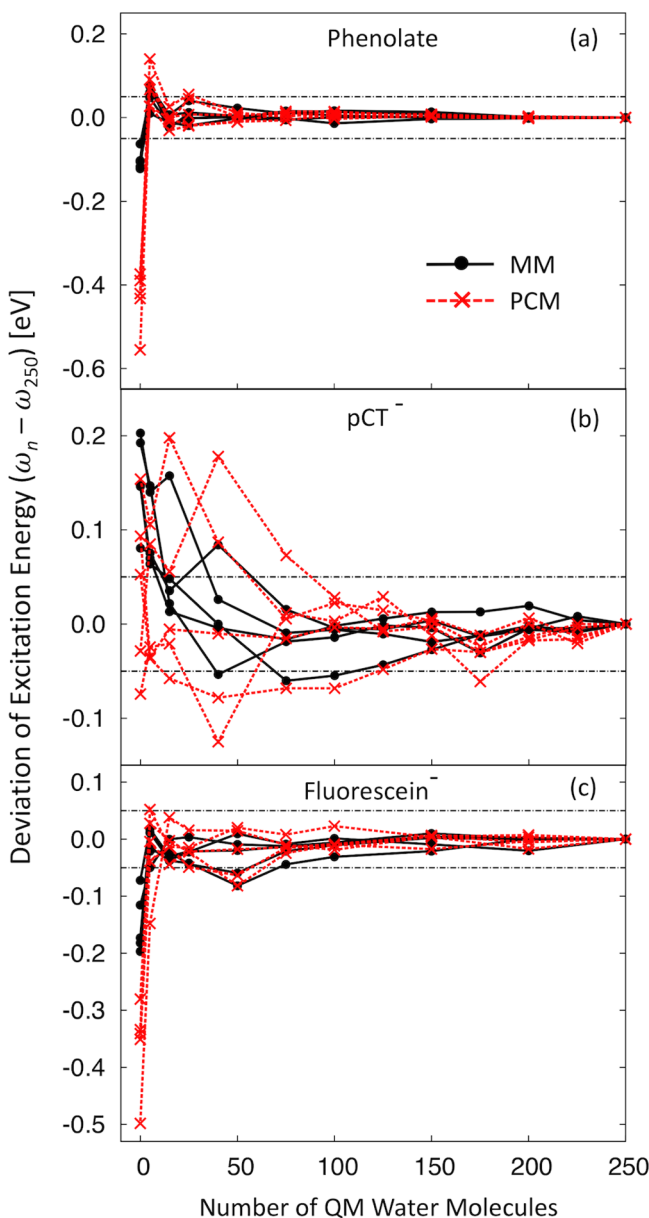


Figure 6. Deviation of QM/classical excitation energies from the values computed with 250 QM water molecules ($\omega_n - \omega_{250}$) for five snapshots of (a) phenolate, (b) pCT^- , and (c) the fluorescein anion. The classical region is modeled by TIP3P point charges (MM) or PCM with an SES cavity (PCM). The black dashed-dotted lines indicate deviation of ± 0.05 eV from the values computed with 250 QM water molecules.

have an average absolute deviation of only 0.08 eV, but as the QM region is increased from 5 to 75 QM water molecules, these excitation energies have large deviations (>0.10 eV) both above and below the converged values. The QM/PCM transition dipole moments also show large deviations with respect to values computed with 250 QM water molecules when only part of the first solvation shell is treated with QM (see Figure S5), indicating that the TDDFT eigenvectors are not converged. For most snapshots, the QM/PCM excitation energies are converged to within 0.05 eV of the values computed with 250 QM water molecules when 100–125 water molecules are treated with QM, but the PCM induces a large deviation in excitation energy of -0.06 eV for one snapshot with 175 QM water molecules, which is nearly two full solvation shells.

Overall, our analysis shows that for nearly all solutes and amounts of QM solvent, the QM/MM model is a better choice than the QM/PCM model. For the phenolate and fluorescein anions with no QM solvent, both QM/MM and QM/PCM underestimate the excitation energies, with the error being more substantial with QM/PCM. This is consistent with the amount of charge transfer to QM solvent (see Figure S3). For all solutes with less than a full solvation shell, the QM/MM excitation energies are similar to or are more accurate than the QM/PCM excitation energies. In general, we find that a larger QM region is necessary to converge QM/classical excitation energies when a PCM is used instead of MM point charges. The QM/PCM calculations are computationally more demanding than QM/MM due to the additional PCM routines that self-consistently solve for the apparent surface charges induced by the QM density at the boundary of the PCM cavity. For example, the average CPU time of TDDFT QM/MM calculations of pCT^- with 100 QM water molecules that solve for the lowest energy transition (*nstates* = 1) is 7.4 h compared to 47.9 h for TDDFT QM/PCM calculations. Therefore, it is recommended to use MM point charges to save computational time and to use at least one full QM solvation shell to obtain reasonably converged QM/classical excitation energies.

CONCLUSIONS

Combined QM/classical methods are useful computational tools for modeling the effects of solvent on excitation energies. To obtain accurate excitation energies in solution, one must consider the ability of the excited-state methodology to capture the electronic structure of the solute and solvent, the accuracy of the solute–solvent configurations used for the excited-state calculations, and the quality of the solvent model. Here we focused on the latter aspect necessary for achieving accurate condensed-phase excitation energies.

In this work, we investigated the convergence of QM/classical excitation energies with respect to the size of the QM region for three neutral molecules of increasing molecular size and their anions. In general, about one solvation shell must be included in the QM region to converge the QM/classical excitation energy to within 0.05 eV of the value computed with 250 QM water molecules. Although six solutes of differing character have been explored in this work, cases can likely be found where smaller amounts or larger amounts of QM solvent are necessary to reach convergence of the excitation energy within 0.05 eV. Care should be taken especially with solutes that have energy gaps aligned with the solvent, which can lead to mixing of the solute and solvent wavefunctions and therefore slower convergence. However, our work shows that one should generally go beyond inclusion of only the hydrogen-bonded water molecules in the QM region while computing aqueous excitation energies.

For QM/MM, the well-parameterized atomic point charges of the TIP3P and SPC/E water models give better convergence than both scaled point charges and those derived from QM charge densities using the CHELPG scheme. For QM regions with large amounts of explicit solvent, the PCM cavity must be chosen with care. We found that the default VDW cavity leads to bulk dielectric treatment of the solvent at points on the cavity surface between QM solvent molecules. This nonphysical representation of the solvent converges QM/PCM excitation energies to different values than QM/MM excitation energies. Using the SES definition of the PCM cavity, QM/PCM calculations converge to the same excitation energies as QM/MM calculations and require a similar or larger number of QM

solvent molecules to achieve the same level of convergence as QM/MM calculations. Overall, we found that including mutual polarization between the QM and classical regions through a PCM is computationally more demanding than using an MM environment, but does not improve convergence of excitation energies with respect to the QM region size.

■ ASSOCIATED CONTENT

S Supporting Information

The Supporting Information is available free of charge on the ACS Publications website at DOI: [10.1021/acs.jpcb.6b09176](https://doi.org/10.1021/acs.jpcb.6b09176).

Comparison of density functionals and basis sets for QM/MM excitation energies of a single snapshot of pCT⁻; comparison of MM point charge models for QM/MM excitation energies of five snapshots of pCT⁻; average absolute charge transferred to QM water molecules upon excitation for all solutes with QM/MM and QM/PCM; convergence of excitation energies, transition dipole moments, and oscillator strengths for five snapshots of pCT and five snapshots of pCT⁻ with QM/MM and QM/PCM ([PDF](#))

■ AUTHOR INFORMATION

Corresponding Author

*E-mail: cisborn@ucmerced.edu. Phone: 209-228-4693.

ORCID

Christine M. Isborn: [0000-0002-4905-9113](https://orcid.org/0000-0002-4905-9113)

Author Contributions

All authors have given approval to the final version of the manuscript.

Notes

The authors declare no competing financial interest.

■ ACKNOWLEDGMENTS

The authors would like to thank Prof. Marco Caricato, Dr. Giovanni Scalmani, and Dr. Michael Frisch for discussion about the definitions of PCM cavities available in Gaussian09. Acknowledgement is made to the donors of the American Chemical Society Petroleum Research Fund for supporting the early stages of this research comparing convergence of the QM/MM and QM/PCM methods, under Award Number 53674-DNI6. The later stages of this research, including studies of the PCM cavity, were supported by the Department of Energy, Office of Basic Energy Sciences CTC and CPIMS programs, under Award Number DE-SC0014437. M.R.P. acknowledges the University of California Merced Chancellor's Postdoctoral Fellowship Program for financial support. C. X. was supported through the ACS Project SEED program. We acknowledge computing time on the Multi-Environment Computer for Exploration and Discovery (MERCED) cluster which is supported by National Science Foundation Grant No. ACI-1429783.

■ REFERENCES

- (1) Reichardt, C. Solvatochromic Dyes as Solvent Polarity Indicators. *Chem. Rev.* **1994**, *94*, 2319–2358.
- (2) Marini, A.; Muñoz-Losa, A.; Biancardi, A.; Mennucci, B. What Is Solvatochromism? *J. Phys. Chem. B* **2010**, *114*, 17128–17135.
- (3) Warshel, A.; Levitt, M. Theoretical Studies of Enzymic Reactions: Dielectric, Electrostatic and Steric Stabilization of the Carbonium Ion in the Reaction of Lysozyme. *J. Mol. Biol.* **1976**, *103*, 227–249.

(4) Field, M. J.; Bash, P. A.; Karplus, M. A Combined Quantum Mechanical and Molecular Mechanical Potential for Molecular Dynamics Simulations. *J. Comput. Chem.* **1990**, *11*, 700–733.

(5) Gao, J. Hybrid Quantum and Molecular Mechanical Simulations: An Alternative Avenue to Solvent Effects in Organic Chemistry. *Acc. Chem. Res.* **1996**, *29*, 298–305.

(6) Lin, H.; Truhlar, D. G. QM/MM: What Have We Learned, Where Are We, and Where Do We Go from Here? *Theor. Chem. Acc.* **2007**, *117*, 185–199.

(7) Rivail, J.-L.; Rinaldi, D. A Quantum Chemical Approach to Dielectric Solvent Effects in Molecular Liquids. *Chem. Phys.* **1976**, *18*, 233–242.

(8) Miertuš, S.; Scrocco, E.; Tomasi, J. Electrostatic Interaction of a Solute with a Continuum. A Direct Utilization of AB Initio Molecular Potentials for the Revision of Solvent Effects. *Chem. Phys.* **1981**, *55*, 117–129.

(9) Cramer, C. J.; Truhlar, D. G. Implicit Solvation Models: Equilibria, Structure, Spectra, and Dynamics. *Chem. Rev.* **1999**, *99*, 2161–2200.

(10) Tomasi, J.; Mennucci, B.; Cammi, R. Quantum Mechanical Continuum Solvation Models. *Chem. Rev.* **2005**, *105*, 2999–3093.

(11) Senn, H. M.; Thiel, W. QM/MM Studies of Enzymes. *Curr. Opin. Chem. Biol.* **2007**, *11*, 182–187.

(12) Senn, H. M.; Thiel, W. QM/MM Methods for Biomolecular Systems. *Angew. Chem., Int. Ed. Engl.* **2009**, *48*, 1198–1229.

(13) Acevedo, O.; Jorgensen, W. L. Advances in Quantum and Molecular Mechanical (QM/MM) Simulations for Organic and Enzymatic Reactions. *Acc. Chem. Res.* **2010**, *43*, 142–151.

(14) Shaik, S.; Cohen, S.; Wang, Y.; Chen, H.; Kumar, D.; Thiel, W. P450 Enzymes: Their Structure, Reactivity, and Selectivity-Modeled by QM/MM Calculations. *Chem. Rev.* **2010**, *110*, 949–1017.

(15) Hu, L.; Söderhjelm, P.; Ryde, U. On the Convergence of QM/MM Energies. *J. Chem. Theory Comput.* **2011**, *7*, 761–777.

(16) Liao, R.-Z.; Thiel, W. Convergence in the QM-Only and QM/MM Modeling of Enzymatic Reactions: A Case Study for Acetylene Hydratase. *J. Comput. Chem.* **2013**, *34*, 2389–2397.

(17) Bravaya, K. B.; Grigorenko, B. L.; Nemukhin, A. V.; Krylov, A. I. Quantum Chemistry behind Bioimaging: Insights from Ab Initio Studies of Fluorescent Proteins and Their Chromophores. *Acc. Chem. Res.* **2012**, *45*, 265–275.

(18) Murugan, N. A.; Jha, P. C.; Rinkevicius, Z.; Ruud, K.; Ågren, H. Solvatochromic Shift of Phenol Blue in Water from a Combined Car-Parrinello Molecular Dynamics Hybrid Quantum Mechanics-Molecular Mechanics and ZINDO Approach. *J. Chem. Phys.* **2010**, *132*, No. 234508.

(19) Preat, J.; Jacquemin, D.; Perpète, E. A. A UV/VIS Spectra Investigation of pH-Sensitive Dyes Using Time-Dependent Density Functional Theory. *Int. J. Quantum Chem.* **2010**, *110*, 2147–2154.

(20) Sakata, T.; Kawashima, Y.; Nakano, H. Solvent Effect on the Absorption Spectra of Coumarin 120 in Water: A Combined Quantum Mechanical and Molecular Mechanical Study. *J. Chem. Phys.* **2011**, *134*, No. 014501.

(21) Isborn, C. M.; Götz, A. W.; Clark, M. A.; Walker, R. C.; Martínez, T. J. Electronic Absorption Spectra from MM and Ab Initio QM/MM Molecular Dynamics: Environmental Effects on the Absorption Spectrum of Photoactive Yellow Protein. *J. Chem. Theory Comput.* **2012**, *8*, 5092–5106.

(22) Ma, H.; Ma, Y. Solvent Effect on Electronic Absorption, Fluorescence, and Phosphorescence of Acetone in Water: Revisited by Quantum Mechanics/molecular Mechanics (QM/MM) Simulations. *J. Chem. Phys.* **2013**, *138*, No. 224505.

(23) Retegan, M.; Neese, F.; Pantazis, D. A. Convergence of QM/MM and Cluster Models for the Spectroscopic Properties of the Oxygen-Evolving Complex in Photosystem II. *J. Chem. Theory Comput.* **2013**, *9*, 3832–3842.

(24) Valsson, O.; Campomanes, P.; Tavernelli, I.; Rothlisberger, U.; Filippi, C. Rhodopsin Absorption from First Principles: Bypassing Common Pitfalls. *J. Chem. Theory Comput.* **2013**, *9*, 2441–2454.

- (25) Amat, P.; Nifosi, R. Spectral “Fine” Tuning in Fluorescent Proteins: The Case of the GFP-Like Chromophore in the Anionic Protonation State. *J. Chem. Theory Comput.* **2013**, *9*, 497–508.
- (26) Gao, J.; Shi, W.-J.; Ye, J.; Wang, X.; Hirao, H.; Zhao, Y. QM/MM Modeling of Environmental Effects on Electronic Transitions of the FMO Complex. *J. Phys. Chem. B* **2013**, *117*, 3488–3495.
- (27) Tazhigulov, R. N.; Bravaya, K. B. Free Energies of Redox Half-Reactions from First-Principles Calculations. *J. Phys. Chem. Lett.* **2016**, *7*, 2490–2495.
- (28) Thole, B. T. Molecular Polarizabilities Calculated with a Modified Dipole Interaction. *Chem. Phys.* **1981**, *59*, 341–350.
- (29) Curutchet, C.; Muñoz-Losa, A.; Monti, S.; Kongsted, J.; Scholes, G. D.; Mennucci, B. Electronic Energy Transfer in Condensed Phase Studied by a Polarizable QM/MM Model. *J. Chem. Theory Comput.* **2009**, *5*, 1838–1848.
- (30) Olsen, J. M.; Aidas, K.; Kongsted, J. Excited States in Solution through Polarizable Embedding. *J. Chem. Theory Comput.* **2010**, *6*, 3721–3734.
- (31) Rick, S. W.; Berne, B. J. Dynamical Fluctuating Charge Force Fields: The Aqueous Solvation of Amides. *J. Am. Chem. Soc.* **1996**, *118*, 672–679.
- (32) Lamoureux, G.; Roux, B. Modeling Induced Polarization with Classical Drude Oscillators: Theory and Molecular Dynamics Simulation Algorithm. *J. Chem. Phys.* **2003**, *119*, 3025.
- (33) Dreuw, A.; Head-Gordon, M. Single-Reference Ab Initio Methods for the Calculation of Excited States of Large Molecules. *Chem. Rev.* **2005**, *105*, 4009–4037.
- (34) Casida, M. E. Time-Dependent Density-Functional Theory for Molecules and Molecular Solids. *J. Mol. Struct.: THEOCHEM* **2009**, *914*, 3–18.
- (35) Dreuw, A.; Weisman, J. L.; Head-Gordon, M. Long-Range Charge-Transfer Excited States in Time-Dependent Density Functional Theory Require Non-Local Exchange. *J. Chem. Phys.* **2003**, *119*, 2943.
- (36) Tozer, D. J. Relationship between Long-Range Charge-Transfer Excitation Energy Error and Integer Discontinuity in Kohn–Sham Theory. *J. Chem. Phys.* **2003**, *119*, 12697.
- (37) Bernasconi, L.; Sprik, M.; Hutter, J. Time Dependent Density Functional Theory Study of Charge-Transfer and Intramolecular Electronic Excitations in Acetone–water Systems. *J. Chem. Phys.* **2003**, *119*, 12417.
- (38) Neugebauer, J.; Gritsenko, O.; Baerends, E. J. Assessment of a Simple Correction for the Long-Range Charge-Transfer Problem in Time-Dependent Density-Functional Theory. *J. Chem. Phys.* **2006**, *124*, No. 214102.
- (39) Lange, A.; Herbert, J. M. Simple Methods To Reduce Charge-Transfer Contamination in Time-Dependent Density-Functional Calculations of Clusters and Liquids. *J. Chem. Theory Comput.* **2007**, *3*, 1680–1690.
- (40) Isborn, C. M.; Mar, B. D.; Curchod, B. F. E.; Tavernelli, I.; Martínez, T. J. The Charge Transfer Problem in Density Functional Theory Calculations of Aqueously Solvated Molecules. *J. Phys. Chem. B* **2013**, *117*, 12189–12201.
- (41) Tawada, Y.; Tsuneda, T.; Yanagisawa, S.; Yanai, T.; Hirao, K. A Long-Range-Corrected Time-Dependent Density Functional Theory. *J. Chem. Phys.* **2004**, *120*, 8425.
- (42) Gritsenko, O.; Baerends, E. J. Asymptotic Correction of the Exchange–correlation Kernel of Time-Dependent Density Functional Theory for Long-Range Charge-Transfer Excitations. *J. Chem. Phys.* **2004**, *121*, 655.
- (43) Rohrdanz, M. A.; Martins, K. M.; Herbert, J. M. A Long-Range-Corrected Density Functional That Performs Well for Both Ground-State Properties and Time-Dependent Density Functional Theory Excitation Energies, Including Charge-Transfer Excited States. *J. Chem. Phys.* **2009**, *130*, No. 054112.
- (44) Eilmes, A. Solvatochromic Probe in Molecular Solvents: Implicit versus Explicit Solvent Model. *Theor. Chem. Acc.* **2014**, *133*, 1538.
- (45) Pavone, M.; Brancato, G.; Morelli, G.; Barone, V. Spectroscopic Properties in the Liquid Phase: Combining High-Level Ab Initio Calculations and Classical Molecular Dynamics. *ChemPhysChem* **2006**, *7*, 148–156.
- (46) Aidas, K.; Møgelholj, A.; Nilsson, E. J. K.; Johnson, M. S.; Mikkelsen, K. V.; Christiansen, O.; Söderhjelm, P.; Kongsted, J. On the Performance of Quantum Chemical Methods to Predict Solvatochromic Effects: The Case of Acrolein in Aqueous Solution. *J. Chem. Phys.* **2008**, *128*, No. 194503.
- (47) Chandrasekaran, S.; Aghtar, M.; Valleau, S.; Aspuru-Guzik, A.; Kleinekathöfer, U. Influence of Force Fields and Quantum Chemistry Approach on Spectral Densities of BChl a in Solution and in FMO Proteins. *J. Phys. Chem. B* **2015**, *119*, 9995–10004.
- (48) Marenich, A. V.; Cramer, C. J.; Truhlar, D. G. Sorting Out the Relative Contributions of Electrostatic Polarization, Dispersion, and Hydrogen Bonding to Solvatochromic Shifts on Vertical Electronic Excitation Energies. *J. Chem. Theory Comput.* **2010**, *6*, 2829–2844.
- (49) Pedone, A.; Bloino, J.; Monti, S.; Prampolini, G.; Barone, V. Absorption and Emission UV-Vis Spectra of the TRITC Fluorophore Molecule in Solution: A Quantum Mechanical Study. *Phys. Chem. Chem. Phys.* **2010**, *12*, 1000–1006.
- (50) Zuehlsdorff, T. J.; Haynes, P. D.; Hanke, F.; Payne, M. C.; Hine, N. D. M. Solvent Effects on Electronic Excitations of an Organic Chromophore. *J. Chem. Theory Comput.* **2016**, *12*, 1853–1861.
- (51) Klamt, A.; Schüürmann, G. COSMO: A New Approach to Dielectric Screening in Solvents with Explicit Expressions for the Screening Energy and Its Gradient. *J. Chem. Soc., Perkin Trans. 2* **1993**, *799*–805.
- (52) Stefanovich, E. V.; Truong, T. N. Optimized Atomic Radii for Quantum Dielectric Continuum Solvation Models. *Chem. Phys. Lett.* **1995**, *244*, 65–74.
- (53) Klamt, A. Conductor-like Screening Model for Real Solvents: A New Approach to the Quantitative Calculation of Solvation Phenomena. *J. Phys. Chem.* **1995**, *99*, 2224–2235.
- (54) Barone, V.; Cossi, M. Quantum Calculation of Molecular Energies and Energy Gradients in Solution by a Conductor Solvent Model. *J. Phys. Chem. A* **1998**, *102*, 1995–2001.
- (55) Cossi, M.; Rega, N.; Scalmani, G.; Barone, V. Energies, Structures, and Electronic Properties of Molecules in Solution with the C-PCM Solvation Model. *J. Comput. Chem.* **2003**, *24*, 669–681.
- (56) Pye, C. C.; Ziegler, T. An Implementation of the Conductor-like Screening Model of Solvation within the Amsterdam Density Functional Package. *Theor. Chem. Acc.* **1999**, *101*, 396–408.
- (57) Frisch, M. J.; Trucks, G. W.; Schlegel, H. B.; Scuseria, G. E.; Robb, M. A.; Cheeseman, J. R.; Scalmani, G.; Barone, V.; Mennucci, B.; Petersson, G. A.; et al. *Gaussian 09*, revision D.01; Gaussian, Inc.: Wallingford, CT, 2013.
- (58) Rappe, A. K.; Casewit, C. J.; Colwell, K. S.; Goddard, W. A.; Skiff, W. M. UFF, a Full Periodic Table Force Field for Molecular Mechanics and Molecular Dynamics Simulations. *J. Am. Chem. Soc.* **1992**, *114*, 10024–10035.
- (59) Marenich, A. V.; Cramer, C. J.; Truhlar, D. G. Universal Solvation Model Based on Solute Electron Density and on a Continuum Model of the Solvent Defined by the Bulk Dielectric Constant and Atomic Surface Tensions. *J. Phys. Chem. B* **2009**, *113*, 6378–6396.
- (60) Connolly, M. L. Solvent-Accessible Surfaces of Proteins and Nucleic Acids. *Science* **1983**, *221*, 709–713.
- (61) Connolly, M. L. Analytical Molecular Surface Calculation. *J. Appl. Crystallogr.* **1983**, *16*, 548–558.
- (62) Wong, M. W.; Wiberg, K. B.; Frisch, M. J. Ab Initio Calculation of Molar Volumes: Comparison with Experiment and Use in Solvation Models. *J. Comput. Chem.* **1995**, *16*, 385–394.
- (63) Foresman, J. B.; Keith, T. A.; Wiberg, K. B.; Snoonian, J.; Frisch, M. J. Solvent Effects. 5. Influence of Cavity Shape, Truncation of Electrostatics, and Electron Correlation on Ab Initio Reaction Field Calculations. *J. Phys. Chem.* **1996**, *100*, 16098–16104.
- (64) Scherlis, D. A.; Fattebert, J.-L.; Gygi, F.; Cococcioni, M.; Marzari, N. A Unified Electrostatic and Cavitation Model for First-Principles Molecular Dynamics in Solution. *J. Chem. Phys.* **2006**, *124*, 074103.
- (65) Casida, M. E. Time-Dependent Density Functional Response Theory for Molecules. In *Recent Advances in Density Functional Methods*;

- Chong, D. P., Ed.; Recent Advances in Computational Chemistry; World Scientific, 1995; Vol. 1, pp 155–192.
- (66) Ullrich, C. *Time-Dependent Density-Functional Theory: Concepts and Applications*; Oxford University Press: Oxford; New York, 2012.
- (67) Iozzi, M. F.; Mennucci, B.; Tomasi, J.; Cammi, R. Excitation Energy Transfer (EET) between Molecules in Condensed Matter: A Novel Application of the Polarizable Continuum Model (PCM). *J. Chem. Phys.* **2004**, *120*, 7029.
- (68) Cammi, R.; Mennucci, B.; Tomasi, J. Fast Evaluation of Geometries and Properties of Excited Molecules in Solution: A Tamm-Danoff Model with Application to 4-Dimethylaminobenzonitrile. *J. Phys. Chem. A* **2000**, *104*, 5631–5637.
- (69) Case, D. A.; Darden, T. A.; Cheatham, T. E., III; Simmerling, C. L.; Wang, J.; Duke, R. E.; Luo, R.; Walker, R. C.; Zhang, W.; Merz, K. M.; et al. AMBER 12; University of California San Francisco: San Francisco, CA, 2012.
- (70) Wang, J.; Wang, W.; Kollman, P. A.; Case, D. A. Automatic Atom Type and Bond Type Perception in Molecular Mechanical Calculations. *J. Mol. Graphics Modell.* **2006**, *25*, 247–260.
- (71) Wang, J.; Wolf, R. M.; Caldwell, J. W.; Kollman, P. A.; Case, D. A. Development and Testing of a General AMBER Force Field. *J. Comput. Chem.* **2004**, *25*, 1157–1174.
- (72) Jorgensen, W. L.; Chandrasekhar, J.; Madura, J. D.; Impey, R. W.; Klein, M. L. Comparison of Simple Potential Functions for Simulating Liquid Water. *J. Chem. Phys.* **1983**, *79*, 926.
- (73) Hirata, S.; Head-Gordon, M. Time-Dependent Density Functional Theory within the Tamm–Danoff Approximation. *Chem. Phys. Lett.* **1999**, *314*, 291–299.
- (74) Cancès, E.; Mennucci, B.; Tomasi, J. A New Integral Equation Formalism for the Polarizable Continuum Model: Theoretical Background and Applications to Isotropic and Anisotropic Dielectrics. *J. Chem. Phys.* **1997**, *107*, 3032.
- (75) Tomasi, J.; Mennucci, B.; Cancès, E. The IEF Version of the PCM Solvation Method: An Overview of a New Method Addressed to Study Molecular Solutes at the QM Ab Initio Level. *J. Mol. Struct.: THEOCHEM* **1999**, *464*, 211–226.
- (76) Breneman, C. M.; Wiberg, K. B. Determining Atom-Centered Monopoles from Molecular Electrostatic Potentials. The Need for High Sampling Density in Formamide Conformational Analysis. *J. Comput. Chem.* **1990**, *11*, 361–373.
- (77) Chai, J.-D.; Head-Gordon, M. Systematic Optimization of Long-Range Corrected Hybrid Density Functionals. *J. Chem. Phys.* **2008**, *128*, No. 084106.
- (78) Zhao, Y.; Truhlar, D. G. The M06 Suite of Density Functionals for Main Group Thermochemistry, Thermochemical Kinetics, Non-covalent Interactions, Excited States, and Transition Elements: Two New Functionals and Systematic Testing of Four M06-Class Functionals and 12 Other Function. *Theor. Chem. Acc.* **2008**, *120*, 215–241.
- (79) Zhao, Y.; Truhlar, D. G. Density Functional for Spectroscopy: No Long-Range Self-Interaction Error, Good Performance for Rydberg and Charge-Transfer States, and Better Performance on Average than B3LYP for Ground States. *J. Phys. Chem. A* **2006**, *110*, 13126–13130.
- (80) Vydrov, O. A.; Scuseria, G. E. Assessment of a Long-Range Corrected Hybrid Functional. *J. Chem. Phys.* **2006**, *125*, No. 234109.
- (81) Chai, J.-D.; Head-Gordon, M. Long-Range Corrected Hybrid Density Functionals with Damped Atom-Atom Dispersion Corrections. *Phys. Chem. Chem. Phys.* **2008**, *10*, 6615–6620.
- (82) Grimme, S.; Antony, J.; Ehrlich, S.; Krieg, H. A Consistent and Accurate Ab Initio Parametrization of Density Functional Dispersion Correction (DFT-D) for the 94 Elements H–Pu. *J. Chem. Phys.* **2010**, *132*, No. 154104.
- (83) Berendsen, H. J. C.; Grigera, J. R.; Straatsma, T. P. The missing term in effective pair potentials. *J. Phys. Chem.* **1987**, *91*, 6269–6271.